

# Extracting the Wavefunction of the LSP at the LHC

Gordon Kane<sup>a</sup>, Eric Kuflik<sup>a</sup>, and Brent D. Nelson<sup>b</sup>

(a) *Michigan Center for Theoretical Physics, University of Michigan, Ann Arbor, MI 48109, USA*

(b) *Department of Physics, Northeastern University, Boston, MA 02115, USA*

(Dated: June 2, 2019)

We consider associated production of squarks and gluinos with the lightest supersymmetric particle (LSP), or states nearly degenerate in mass with it. Though sub-dominant to pair production of color  $SU(3)$ -charged superpartners, these processes are directly sensitive to the wavefunction composition of the lightest neutralinos. Exploiting event-shape variables – including some introduced here for the first time – we are able to identify the composition of the LSP by selecting events involving a single high- $p_T$  jet recoiling against missing transverse energy. We illustrate the proposed technique on a set of benchmark cases and propose methods for applying these results in more realistic experimental environments.

## I. INTRODUCTION: GENERAL GOALS

With the LHC experiments currently collecting data it is not inconceivable that a discovery of low-energy supersymmetry could be made in the near future. The subsequent months and years will be spent making numerous measurements of masses, cross-sections and branching ratios. As was emphasized in earlier work [1], for the theorist trying to reconstruct the underlying supersymmetric Lagrangian and looking for clues as to the origin of supersymmetry breaking, this information is useful only to the extent that it can (uniquely) determine the soft supersymmetry breaking parameters themselves. Of these, it has been argued that the soft masses of the gauginos are particularly important for distinguishing between high-scale models of supersymmetry breaking [2]. In recent work a subset of the authors demonstrated how a synthetic approach that considers an ensemble of targeted observables can be used to perform a fit to the ratios of gaugino masses [3]. Here we would like to turn our attention to the other great unknown of the gaugino sector: the composition of the wavefunction of the lightest neutralino.

It has long been appreciated that in the R-parity conserving minimal supersymmetric Standard Model (MSSM), the lightest supersymmetric particle (LSP) will be stable and can therefore provide a good dark matter candidate if it is uncolored and electrically neutral [4]. Assuming that this LSP is the lightest mass eigenstate of the neutralino system, then the cosmological properties of this state will be highly dependent on the composition of its wavefunction. For example, the question of whether the thermally-produced relic density of the LSP is sufficient to account for the known non-baryonic dark matter – or whether some non-thermal production mechanisms will be needed – is crucially sensitive to the wavefunction of the LSP [5]. So too is its scattering rate in terrestrial direct detection experiments [6]. The question becomes even more urgent if the measured excess in the positron composition of cosmic rays [7, 8] is taken to be a signal of new (supersymmetric) physics [9, 10].

Extracting the wavefunction of the LSP from measurements of cross-sections  $\times$  branching fractions is known to be extremely difficult at hadron colliders such as the LHC due to an inability to over-constrain the independent entries in the neutralino mass matrix [11]. The typical strategy therefore in-

volves a global fit to these entries, which typically suffers from a lack of uniqueness (the so called ‘inverse problem’) [12].

In this paper our goals are more modest: we will seek a set of observables which are directly sensitive to the wavefunction composition of the LSP without attempting to reconstruct the full set of eigenvalues and eigenvectors for the neutralino system. The analysis techniques presented here are to be understood as a suggested first step towards a realistic measurement strategy for this important theoretical property. Here we will demonstrate the effectiveness of our analysis technique on test cases based on the highly-studied Snowmass benchmark points [13]. We expect that the techniques we will explore will prove fruitful only after a sizable period of data-taking, and we therefore consider the case of  $\mathcal{O}(10)$  fb<sup>-1</sup> of integrated luminosity at  $\sqrt{s} = 14$  TeV center of mass energies.

In Section II we present a non-technical summary of the basic approach and introduce the benchmark models we will employ as illustration. In Section III we introduce a set of new event-shape variables which will prove crucial to the analysis method which follows. We will use the benchmarks to demonstrate the correlation between LSP wave-function extremes (bino-like versus wino-like versus Higgsino-like) and the event-shape distributions for associated production of a single LSP with  $SU(3)$ -charged superpartners. In Section IV we provide the majority of our results. We will demonstrate how extraction of events with direct production of the LSP, in association with a strongly-coupled superpartner, can be performed with high efficiency from the general superpartner production modes. It will be shown that a combination of distribution shapes and integrated count rates in select channels can distinguish between wavefunction extremes, when other aspects of the superpartner spectra are held fixed. We will indicate how the overall signal can be separated from the Standard Model background at a cursory level – a more detailed treatment of backgrounds will be reserved for a future analysis. Some directions for improving the analysis will be given in the concluding section. The analysis that we are discussing will be done after superpartners are discovered, and their masses are known and can be used to simplify the studies.

	Pure Bino	Pure Wino	Pure Higgsino
$\tilde{N}_1 \tilde{g}$	✓	✓	
$\tilde{N}_1 \tilde{q}_R$	✓		
$\tilde{N}_1 \tilde{q}_L$		✓	
$\tilde{N}_1 \tilde{N}_2$			✓
$\tilde{N}_1 \tilde{C}_1$		✓	✓

TABLE I. Allowed production processes of the form  $\tilde{x} \tilde{N}_1$ , for the pure wavefunction limits. A checkmark means that process is allowed. In this table  $\tilde{q}$  always represents a squark of the first two generations and we assume no mixing between the superpartners of the left- and right-handed quarks.

## II. OVERVIEW OF THE IDEA

In the MSSM the neutralino sector consists of four states whose masses are given (at tree level) by the eigenvalues of the neutralino mass matrix

$$\begin{pmatrix} M_1 & 0 & -s_W c_\beta M_Z & s_W s_\beta M_Z \\ 0 & M_2 & c_W c_\beta M_Z & -c_W s_\beta M_Z \\ -s_W c_\beta M_Z & c_W c_\beta M_Z & 0 & -\mu \\ s_W s_\beta M_Z & -c_W s_\beta M_Z & -\mu & 0 \end{pmatrix}, \quad (1)$$

where  $M_1$  is the soft supersymmetry breaking mass of the hypercharge U(1) gaugino at the electroweak scale,  $M_2$  is the soft supersymmetry breaking mass mass of the SU(2) gauginos at the electroweak scale,  $c_W = \cos \theta_W$  and  $s_W = \sin \theta_W$  involve the weak mixing angle, and  $c_\beta = \cos \beta$  and  $s_\beta = \sin \beta$  involve the ratio of the two Higgs scalar vevs ( $\tan \beta = \langle h_u \rangle / \langle h_d \rangle$ ). The matrix (1) is given in the  $(\tilde{B}, \tilde{W}, \tilde{H}_d^0, \tilde{H}_u^0)$  basis, where  $\tilde{B}$  represents the bino,  $\tilde{W}$  represents the neutral wino and  $\tilde{H}_d^0$  and  $\tilde{H}_u^0$  are the down-type and up-type Higgsinos, respectively.

The mass matrix in (1) is diagonalized by a unitary matrix  $N$  whose entries we will denote by  $N_{ij}$ . The content of the LSP can therefore be parameterized by the expression

$$\tilde{N}_1 = N_{11} \tilde{B} + N_{12} \tilde{W} + N_{13} \tilde{H}_d^0 + N_{14} \tilde{H}_u^0, \quad (2)$$

which is normalized to  $N_{11}^2 + N_{12}^2 + N_{13}^2 + N_{14}^2 = 1$ . Thus in saying that the bino content of the lightest neutralino is high, we mean  $N_{11}^2 \simeq 1$ , for a wino-like LSP we mean  $N_{12}^2 \simeq 1$  and similarly for the Higgsino limit we mean  $N_{13}^2 + N_{14}^2 \simeq 1$ .

Ideally we would like to find a set of observables which will accurately measure each of the entries  $N_{1j}$  without attempting to reconstruct the entire matrix  $N$ . In this paper we will concentrate on distinguishing between the three extreme cases defined in the previous paragraph, reserving a more general treatment (with arbitrary mixtures of various component states) to a future study.

### A. Relevant Processes

To study the wavefunction of the LSP at the LHC it will be necessary to isolate processes that depend strongly on the en-

Channel	$\sigma$ (fb)
$\tilde{N}_1 \tilde{g}$	88.4
$\tilde{N}_1 \tilde{q}_R$	219.3
$\tilde{N}_1 \tilde{q}_L$	18.2
$\tilde{N}_1 \tilde{N}_2$	0.9
$\tilde{N}_1 \tilde{C}_1$	2.7

TABLE II. Production cross sections for processes of Table I for the particular example of SPS point 1A. The total supersymmetric production is  $\sigma_{\text{SUSY}} = 41.5$  pb

tries of the eigenvector  $N_{1j}$ . We therefore consider associated production of the lightest neutralino with other superpartners – particularly the squarks and gluinos, which we will refer to as ‘semi-strong’ production modes. Associated production with other neutralinos and charginos may also be important, and will be discussed in more detail below. Table I lists the allowed production processes  $\tilde{x} \tilde{N}_1$  we will consider for the extreme cases for our neutralino (the limit of 100% bino or wino or Higgsino content). A checkmark indicates that this process is allowed for the particular wavefunction extreme. It is immediately clear from the ‘texture’ in Table I that these processes carry sufficient information to distinguish between the extreme cases. Naturally as one interpolates between extreme cases the entire table is filled out to varying degrees, but here let us focus on the simpler case of understanding the nature of the pure LSP limits. Focusing on the first three lines (the semi-strong production processes), which generally have higher cross-sections than electroweak gaugino pair production, the overall strategy is apparent. If we can make measurements so as to fill in this triplet with one’s and zero’s we would match it to the patterns in Table I and identify the composition of the LSP.

There are, however, a number of issues which complicate matters. The processes in Table I typically have cross-sections which are at least an order of magnitude smaller than dominant processes like gluino pair production or gluino/squark associated production. Thus we expect that the measurements we hope to make require a significant amount of integrated luminosity. For example, the much-studied Snowmass point SPS 1A has a mostly bino-like LSP ( $N_{11}^2 = 0.996$ ) and relatively light gluino ( $m_{\tilde{g}} \sim 600$  GeV). It is therefore an excellent candidate for early discovery at the LHC. Using PYTHIA 6.4 [18] we calculate the total supersymmetric production cross-section to be  $\sigma_{\text{SUSY}} = 41.5$  pb, almost half of which comes from gluino/squark associated production  $\sigma_{\tilde{g}\tilde{q}} = 20.6$  pb. The production cross-sections for the individual sub-processes of Table I are given for SPS point 1A in Table II. Note that these values are given in femtobarns. The semi-strong production mode  $\tilde{N}_1 \tilde{q}_L$  is suppressed relative to the others, but not entirely absent due to the non-vanishing wino-content of the LSP. Note that PYTHIA by default introduces no mixing between the superpartners of the left-handed and right-handed quarks for the first two generations of squarks, which are here denoted by the generic symbol  $\tilde{q}$ . Extracting these subdominant processes from the supersym-

Extreme	Number	Identities
Pure Bino	1	$N_1$
Pure Wino	2	$N_1, C_1$
Pure Higgsino	3	$N_1, C_1, N_2$

TABLE III. Effective number of LSPs producing  $\cancel{E}_T$ , for the extreme wavefunction endpoints. Note that the Higgsino extreme may even have four effective LSPs if we include the  $N_3$ , which is often also close in mass.

metric and Standard Model backgrounds will be challenging, but not impossible, as we will demonstrate in Section IV.

An additional, and more subtle, challenge will be isolating only those cases in which the lightest neutralino  $\tilde{N}_1$  is produced in the semi-strong production process, as opposed to heavier gaugino states. To illustrate, consider the case of an extremely wino-like LSP. To achieve this outcome it is typically necessary to have  $M_2 \ll M_1, \mu$  in the neutralino mass matrix. This simultaneously produces a light chargino  $\tilde{C}_1$  which is then typically nearly degenerate in mass with the lightest neutralino. The phenomenology of this extreme case is very different from the more familiar bino-like extreme for which  $m_{\tilde{N}_2} \simeq m_{\tilde{C}_1}$  with both being significantly more massive than the LSP. The wino-like extreme has been studied extensively in the context of models of anomaly-mediated supersymmetry breaking [19–21] where there are effectively two LSPs since the decay of the lightest chargino to the lightest neutralino involves very soft decay products which are generally not detected. The same analysis can be performed for the case of the Higgsino extreme, for which we require  $\mu \ll M_1, M_2$  and often have three, or even four effective LSPs quite close in mass with one another. This state of affairs is summarized in Table III. In the Higgsino case this is especially vexing as the gauginos  $N_2$  and  $C_1$  may very well appear in semi-strong production processes, even when the true LSP  $N_1$  cannot. As we will investigate in Section IV, this will turn out to be one of the largest difficulties in extracting the wavefunction of the LSP from LHC data.

### B. Benchmark Models

To focus our study we will work with a set of benchmark models, sacrificing some generality for concreteness. Our starting point will be the pair of benchmarks SPS 1A and SPS 2 from the Snowmass benchmark set [13]. These two “base models” are derived from minimal supergravity (mSUGRA) which postulates an overall scalar mass  $m_0$ , overall gaugino mass  $m_{1/2}$  and overall scalar trilinear coupling  $A_0$  at some high energy scale, which then must be evolved to low energies via the renormalization group (RG) equations. The points SPS 1A and SPS 2 are designed to yield opposite hierarchies between the lightest  $SU(3)$ -charged superpartners. Thus SPS 1A has  $m_{\tilde{g}} > m_{\tilde{q}}|_{\min}$  while SPS 2 has  $m_{\tilde{g}} < m_{\tilde{q}}|_{\min}$ , with the lightest squark being a stop in both cases. As we will soon see, heavier squarks will have strong

Base Model	$m_0$	$m_{1/2}$	$A_0$
SPS 1A	100	250	-100
SPS 1A'	1000	250	-100
SPS 2	1450	300	0
SPS 2'	200	300	0

TABLE IV. Input parameters for the four base models. All masses are given in units of GeV and all models have  $\tan \beta = 10$  and  $\mu > 0$ .

Base Model		$M_1$	$M_2$	$\mu$	$m_{N_1}$	$\Delta$	$\Delta^\pm$	Purity	$m_{\tilde{g}}$	$m_{\tilde{t}}$
SPS 1A	Bino	98	300	815	99	203	203	99.6%	602	367
	Wino	300	98	815	101	203	–	99.0%	602	367
	Higgsino	387	815	108	102	14	7	98.0%	602	397
SPS 1A'	Bino	98	300	815	101	211	211	99.6%	654	711
	Wino	300	98	815	103	207	–	99.0%	654	711
	Higgsino	387	815	108	103	13	6	98.1%	654	719
SPS 2	Bino	98	300	815	101	214	214	99.6%	783	979
	Wino	300	98	815	104	207	–	99.0%	783	979
	Higgsino	400	815	108	104	13	6	98.2%	783	983
SPS 2'	Bino	98	300	815	100	206	206	99.6%	714	482
	Wino	300	98	815	101	204	–	99.0%	714	482
	Higgsino	400	815	108	103	13	6	98.1%	715	503

TABLE V. Input Lagrangian masses and physical eigenstate masses for the twelve benchmark points we will consider in what follows. The values of  $\Delta = m_{N_2} - m_{N_1}$  and  $\Delta^\pm = m_{C_1} - m_{N_1}$  reflect the degeneracy in effective LSPs shown in Table III. The LSP mass is kept the same for all the models, so kinematical issues do not confuse the analysis.

implications for the methods we develop in the next section. With this in mind we will develop a variant of each of these two points with the opposite gluino/squark ordering. The set of mSUGRA input parameters for the four benchmarks are given in Table IV, with  $\mu > 0$  and  $\tan \beta = 10$  for all four points.

Over a vast amount of the allowed parameter space of the mSUGRA paradigm the lightest supersymmetric particle is an overwhelmingly bino-like neutralino. The models in Table IV, therefore, provide a good array of superpartner mass patterns but absolutely no variety in the nature of the LSP wavefunction. To remedy this deficiency it will be necessary to modify the input parameters of the neutralino sector from those derived from the values in Table IV. We will do this in such a way as to keep as much of the particle spectrum fixed as is possible, particularly the mass of the lightest eigenstate. Specifically we will choose sets of the input parameters  $\{M_1, M_2, \mu\}$  which achieve at least 98% purity for each of the three wavefunction extremes: bino-like, wino-like and Higgsino-like.

For the bino-like extremes we use values very close to those that arise from the RG evolution of the mSUGRA inputs in Table IV and subsequent requirement of electroweak symmetry breaking:  $M_1 = 98$  GeV,  $M_2 = 300$  GeV and  $\mu = 815$  GeV.

To achieve the wino-like extreme in all four cases it is sufficient to exchange the values of  $M_1$  and  $M_2$  at the electroweak scale. This roughly maintains the mass of the LSP as well as the mass difference  $\Delta = m_{N_2} - m_{N_1}$  between the lightest neutralino and the second lightest eigenstate. Note that this exchange has no effect on the gluino or scalar fermion masses, but the wino-like limit always implies a mass difference between the lightest chargino and the LSP which is vanishingly small  $\Delta^\pm = m_{C_1} - m_{N_1} < 1$  GeV. To achieve the Higgsino-like extreme we set  $M_2 = 815$  GeV at the electroweak scale and then choose the values of  $M_1$  and  $\mu$  according to the approximate formula

$$\mu(M_1) = (3.3 \times 10^{-6} - M_1^{-2.75})^{-1/2.7} \quad (3)$$

in such a way as to keep the LSP mass constant and in agreement with the bino-like and wino-like extremes. In this case both  $\Delta$  and  $\Delta^\pm$  are required to be small but non-vanishing. These values are collected in Table V. Note that changing the value of the  $\mu$ -parameter affects the squark and slepton masses through the off-diagonal mixing terms, but the differences between the masses of these states for each triplet of models is small.

Finally, let us note that the rather large production cross-sections for supersymmetry associated with point SPS 1A may imply that this precise model point has already been excluded by ATLAS and CMS searches for events with jets plus missing transverse energy in the first 35 pb<sup>-1</sup> of data [14–16]. This need not be true, however, of the variants with implied non-universalities in the gaugino sector which we have constructed and listed in Table V [17]. Therefore, given the thorough study these ‘standard candle’ models have received in the literature, and as we will not be discussing discovery of supersymmetry in this work, we will continue to work with the set of models given in Tables IV and V.

### III. EVENT SHAPE VARIABLES

Looking at the semi-strong processes in Table I we see that the production channels that will interest us are ones that will have unbalanced visible energy in the rest frame of the primary collision. If we restrict our attention, therefore, to the transverse plane, event variables which capture this lopsided nature should be helpful in distinguishing these processes from the much more dominant  $\tilde{g}\tilde{g}$  and  $\tilde{g}\tilde{q}$  production.

A widely used and very familiar quantity associated with these types of event-shape variables is *sphericity*,  $s$ , which is defined by [22]

$$S^{ab} = \sum_i p_{ai} p_{bi}, \quad a, b = x, y, z, \quad s = \frac{3}{2} \frac{\lambda_1 \lambda_2}{\text{Tr}(S)} \quad (4)$$

where  $\lambda_1 \leq \lambda_2 \leq \lambda_3$  are the eigenvalues of the matrix  $S$ . When restricted to the transverse plane the relations in (4) become

$$S_T^{ab} = \sum_i p_{ai} p_{bi}, \quad a, b = x, y, \quad s_T = 4 \frac{\text{Det}(S_T)}{\text{Tr}(S_T)^2}. \quad (5)$$

For the processes that will interest us these variables have very similar distributions across all dominant SUSY production channels. It is for this reason that cuts on transverse sphericity are often imposed in inclusive analyses that involve multijet events [23].

To get at our semi-strong processes, therefore, we will need to look beyond the sphericity variables. The next class which will prove useful for our purposes are the *recoil* variables,  $r$ , which are related to observables such as *thrust*. In this paper we will utilize a triplet of such variables, defined by

$$r = \frac{|\sum_i \vec{p}_i|}{\sum_i |\vec{p}_i|} \quad (6)$$

$$r_T = \frac{|\sum_i \vec{p}_{Ti}|}{\sum_i |\vec{p}_{Ti}|} \quad (7)$$

$$r'_T = \frac{E_T}{\sum_i |\vec{p}_{Ti}|}. \quad (8)$$

In addition to the above, we will also introduce a set of new variables,  $q$ ,

$$q = \frac{8/\pi}{(\sum_i |\vec{p}_i|)^2} \sum_{i,j < i} |\vec{p}_i \times \vec{p}_j| \quad (9)$$

$$q_T = \frac{2/\pi}{(\sum_i |\vec{p}_{Ti}|)^2} \sum_{i,j < i} |\vec{p}_{Ti}| |\vec{p}_{Tj}| |(\phi_i - \phi_j)|. \quad (10)$$

We will use the ensemble of twelve models in Table V to demonstrate the efficacy of our shape variables in separating semi-strong production processes from one another and from the remainder of the supersymmetric production processes and the Standard Model backgrounds. We begin by looking at the transverse objects  $r_T$ ,  $r'_T$  and  $q_T$  for the original SPS 1A benchmark (the first model in Table V).

The distributions of these variables are given in Figure 1. The shape variables are formed from the momenta of all *visible* objects in the event, by which we mean that the sum on individual object-level  $p_T$  values does *not* include the missing transverse energy. The supersymmetric data sets in Figure 1 are the total set of all production channels (“All SUSY”) as well as the subset of these which represent  $(N_i/C_i) + (\tilde{q}/\tilde{g})$  associated production (“Semi-Strong”). For the sake of comparison we have generated 5 fb<sup>-1</sup> each of  $t/\bar{t}$  and QCD dijet production at  $\sqrt{s} = 14$  TeV using PYTHIA 6.4 with level one triggers. Distributions for these Standard Model background components are also displayed in Figure 1. All events have been passed to PGS4 to simulate the detector response. Therefore all objects appearing in Figure 1 should be understood as detector objects and not parton-level objects. To make comparison of the relative shapes easier the distributions have been normalized to constant numbers of events.

Each variable is effective at separating semi-strong production channels from the overall supersymmetry signal, though some of the objects defined in equations (6) through (10) are



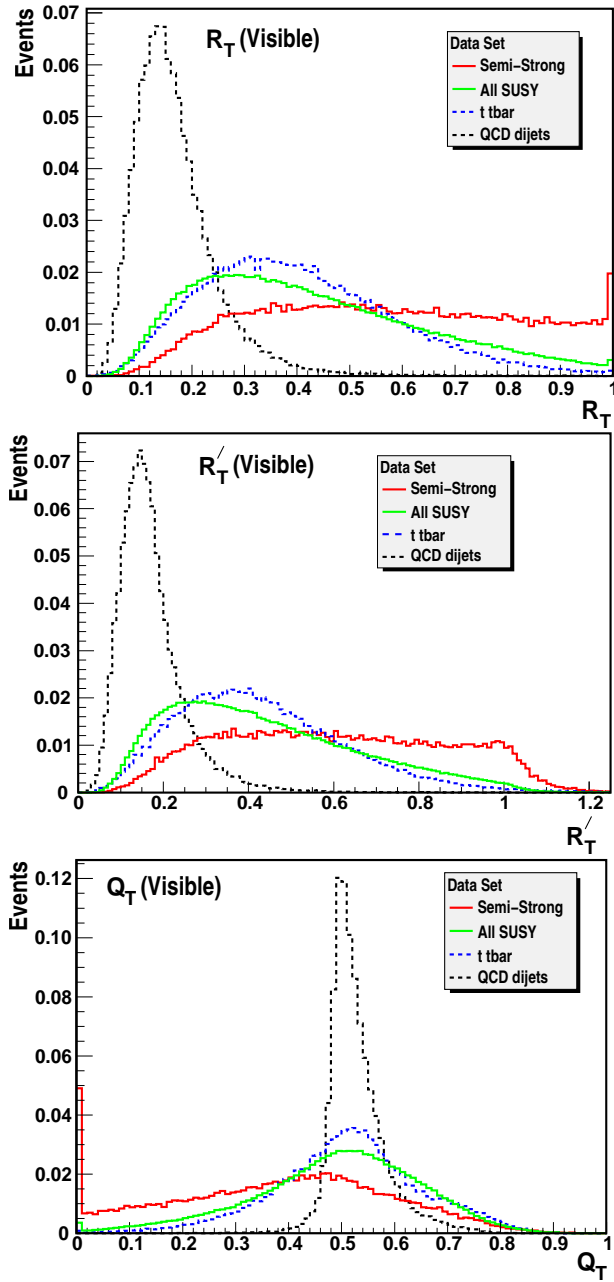


FIG. 1. Distribution of transverse shape variables  $r_T$ ,  $r'_T$  and  $q'_T$  for the bino-like case of point SPS 1A. In each figure the solid lines represent the total SUSY production (thin line) as well as the subset of semi-strong SUSY production channels (heavy line). Distributions are also given for QCD dijet production and  $t, \bar{t}$  pair production. Each plot has been normalized to a constant total number of events.

correlated with one another. In particular the variables  $r_T$  and  $r'_T$  are extremely well correlated, though all other pairs of observables displayed in Figure 1 are only moderately correlated with one another. Note that  $r_T, r'_T \rightarrow 1$  for a single object recoiling against missing energy and vanish for a perfectly spherical/isotropic event, or for two antipodal objects in the event.

By contrast,  $q_T \rightarrow 1/2$  in the antipodal limit,  $2/3$  in the isotropic limit, and vanishes in the single object limit. In fact, for an N-object,  $\mathcal{Z}_N$ -symmetric event

$$q_T = \frac{2}{3} \left( 1 - \frac{1}{N^2} \right). \quad (11)$$

QCD di-jet events typically take on values very close to  $q_T = 1/2$ , but can often be slightly larger if more than two jets are reconstructed in the event. Likewise, distributions for pair produced objects, like gluinos or tops, tend to center around  $q_T = 1/2$ , but can vary depending on the spread of the event. For these reasons, the  $q_T$  variable is an excellent discriminator between semi-strong SUSY events and the backgrounds.

Note that the variable  $r'_T$  is the only one of the variables in (6) through (10) defined to explicitly involve the missing transverse energy. If the energy and momenta of all visible decay products were properly measured we would expect the maximum value of  $r'_T$  to be less than unity. However, the detector simulator PGS4 imposes minimum  $p_T$  requirements for object reconstruction and includes the effect of mismeasurement of object-level  $p_T$ . Therefore the extracted value of  $\cancel{E}_T$  can exceed the sum of the transverse momenta of the ‘visible’ objects in the event, and one finds  $r'_T > 1$ . This is, in fact, what happens in the semi-strong processes which interest us; we shall return to this issue in the next section.

The distributions for these shape variables are qualitatively very similar for the extreme wino-like scenario. In Figure 2 we compare our preferred variables  $r'_T$  and  $q_T$  for the bino and wino extremes of SPS 1a. These correspond to the first two model lines in Table V. The agreement is excellent between the two cases. Once again all distributions have been normalized to equal numbers of events.

#### IV. APPLICATIONS OF EVENT SHAPE VARIABLES

The examples from the previous section clearly indicate that the shape variables from Section III are effective at selecting the sub-dominant contributions from semi-strong associated production of squarks/gluinos and the lightest neutralino. In this section we will outline a procedure for utilizing these variables that is sensitive to the wavefunction composition of the LSP, gradually adding additional realism as we proceed.

As demonstrated in the previous section, the variable  $r'_T$  defined in (8) is one of the more effective shape variables in singling-out the semi-strong production processes. It will therefore play a central role in the analysis outlined below. In Section II we indicated that some of these sub-processes will have an event shape topology very similar to that of the associated production of the LSP neutralino – particularly for the wino-like and Higgsino-like extremes. In Figure 3 we plot the distribution for the variable  $r'_T$  for the combined semi-strong sub-processes and contrast it with the pair production of strongly-coupled superpartners ( $\tilde{g}\tilde{g}$ ,  $\tilde{g}\tilde{q}$  and  $\tilde{q}\tilde{q}$ ) and with the distribution of  $r'_T$  for the Standard Model background. Here we have not taken a sophisticated approach to the background generation, but have instead generated  $5 \text{ fb}^{-1}$  each of  $t/\bar{t}$  and  $b/\bar{b}$  pair production, high- $p_T$  QCD dijet production,

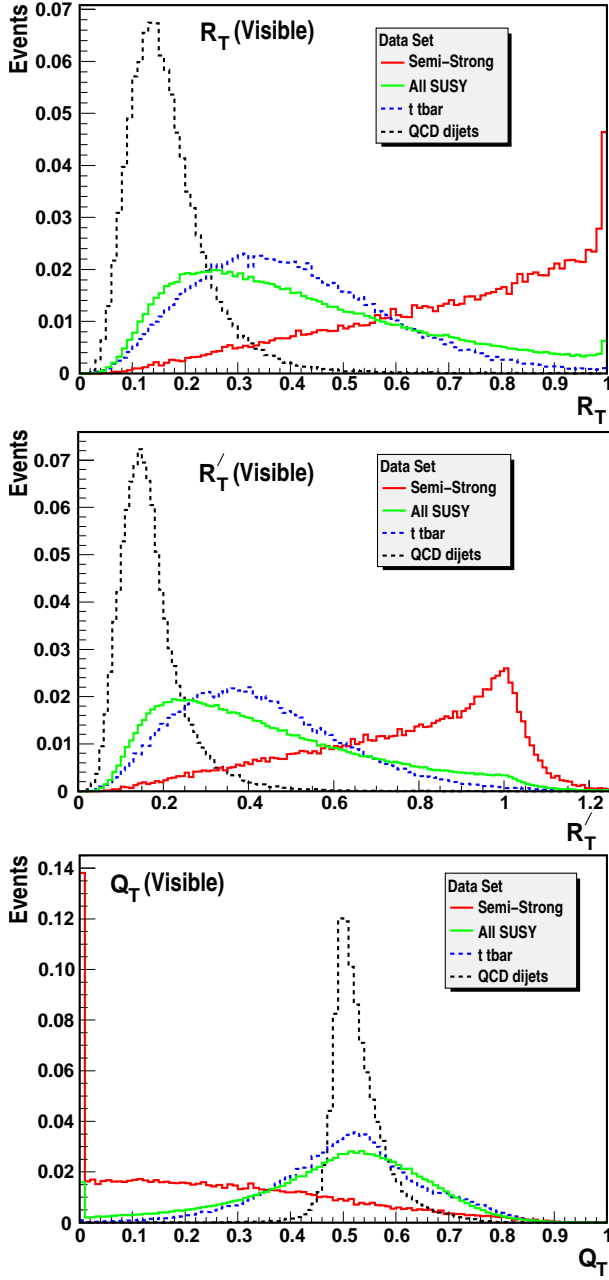


FIG. 2. Distribution of transverse shape variables  $r_T$ ,  $r'_T$  and  $q'_T$  for the wino-like case of point SPS 1A. Plot labeling is identical to Figure 1.

single  $W^\pm$  and  $Z$ -boson production, pair production of electroweak gauge bosons ( $W^+ W^-$ ,  $W^\pm Z$  and  $Z Z$ ), and Drell-Yan processes. Events were generated at  $\sqrt{s} = 14$  TeV using PYTHIA 6.4 with level one triggers.

The region of interest for our purposes is the region where  $r'_T \gtrsim 1$ . We immediately observe that the Standard Model distribution is relatively flat in  $r'_T$ , but a sizeable fraction of the background populates the  $r'_T \geq 1$  bins. Clearly, any procedure for utilizing shape variables to study the wave-function of the LSP will require excellent background rejection. We

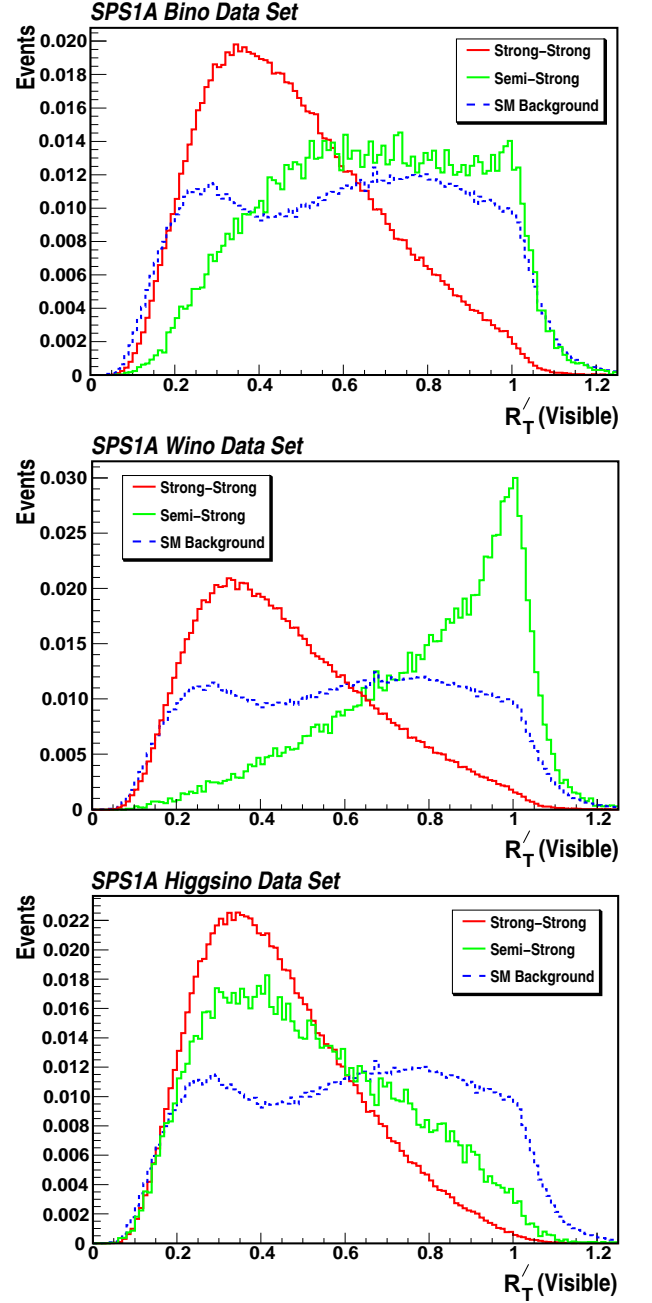


FIG. 3. Distribution of  $r'_T$  shape variable for SPS 1A-based wavefunction extremes. The bino, wino and Higgsino extremes are given in the top, middle and bottom panels, respectively. All data sets involve a single overall cut of  $\cancel{E}_T \geq 175$  GeV and the subsequent data sets have been normalized to constant numbers of events.

will return to this issue shortly. Provided backgrounds can be brought under control, it is clear that the majority of the supersymmetric particle production (represented by the strong-strong data sets) can be well distinguished from the semi-strong processes. In addition, the shape and peak location of these semi-strong distributions (see Figure 2) is clearly influenced by the wavefunction composition of the LSP. As antic-

ipated, the strongest signal for semi-strong production in the  $r'_T \simeq 1$  region occurs for the wino-like extreme, while the weakest signal is the Higgsino-like extreme. For SPS 1A we expect that examination of events with  $r'_T \geq 1$  will clearly distinguish bino-like and wino-like cases from the Higgsino-like case.

The features in these distributions which distinguish between the three wavefunction extremes at large values of  $r'_T$  persist even after all supersymmetric production processes are included in a single dataset. Figure 4 shows the distribution in  $r'_T$  for all SUSY processes for each of the benchmark models in Table V. No event selection cuts have been applied to these distributions, apart from the level one trigger requirements of PGS4, and the distributions are again normalized to constant numbers of events. The wino-like extreme always gives the largest event rate when the curve is integrated from  $r'_T \gtrsim 0.8$  for all four model variants, while the relative sizes of the event rates for the bino-like and Higgsino-like extremes will depend on the mass ordering between the gluinos and the squarks. We note in particular the clear peak in the wino-like distribution for all four cases near  $r'_T \simeq 1$ .

At first glance the results of Figure 4 seem incongruous. If the property  $r'_T \gtrsim 1$  is truly the hallmark of semi-strong production processes, then the simplified discussion in Section II would suggest that the bino-like extreme should give a large number of events in this region for all benchmark models, while the Higgsino-like extreme should be nearly vanishing. Some understanding of the puzzle can be obtained by considering the relative cross-sections for the different components of the total SUSY production for these benchmarks. In Table VI we compare the total SUSY production cross-sections for the three wave-function extremes of points SPS 1A and SPS 2. We further subdivide the total into strong-strong production, semi-strong production (including all charginos and neutralinos) and gaugino-gaugino production of the form  $\tilde{N}_i \tilde{N}_j$ ,  $\tilde{N}_i \tilde{C}_j$  and  $\tilde{C}_i \tilde{C}_j$ . The strong-strong production cross-sections are unaffected by the composition of the neutralinos, as one would expect. But this component accounts for the bulk of the SUSY production processes only for the bino-like extreme for both benchmark points. For the wino-like and Higgsino-like cases the pair-production of electroweak gauginos is a significant component of the total cross-section for SPS 1A events and is the *dominant* component of the SPS 2 total cross-section.

Clearly, then, the shape variable  $r'_T$  is sensitive not only to associated production of strongly-coupled superpartners with electroweak gauginos, but also to electroweak gaugino pair production events. The ‘contamination’ is not as severe as the numbers in Table VI would indicate, however. The bulk of the gaugino pair production events for the wino-like and Higgsino-like extremes involve one or more ‘effective LSP’ states from Table III. The subsequent decays involve soft leptons or jets. Therefore many fail to pass the level one trigger requirements. Trigger efficiencies surpass 90% for all strong-strong and semi-strong processes, but fall to 7-8% for electroweak gaugino production for the wino-like and Higgsino-like extremes of both SPS 1A and SPS 2. After applying the trigger efficiencies the electroweak gaugino pair produc-

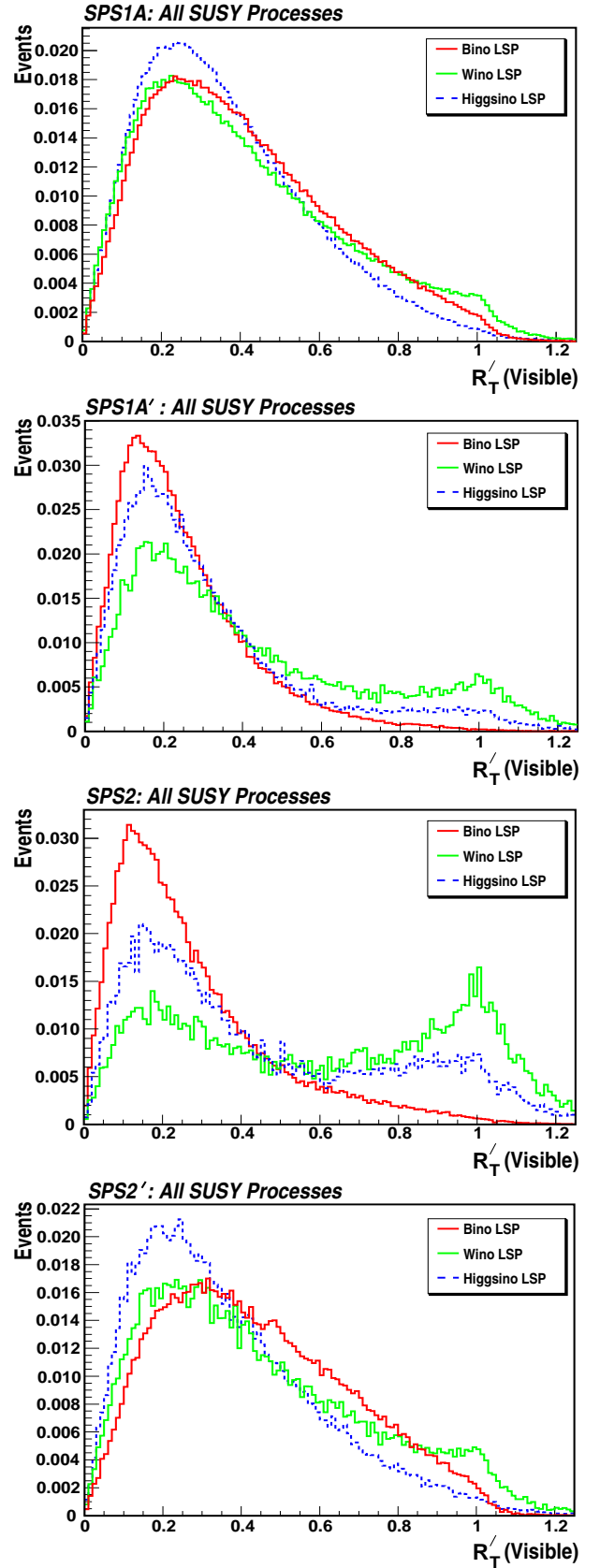


FIG. 4. Distribution of  $r'_T$  shape variable for SPS-based benchmarks of Table V.

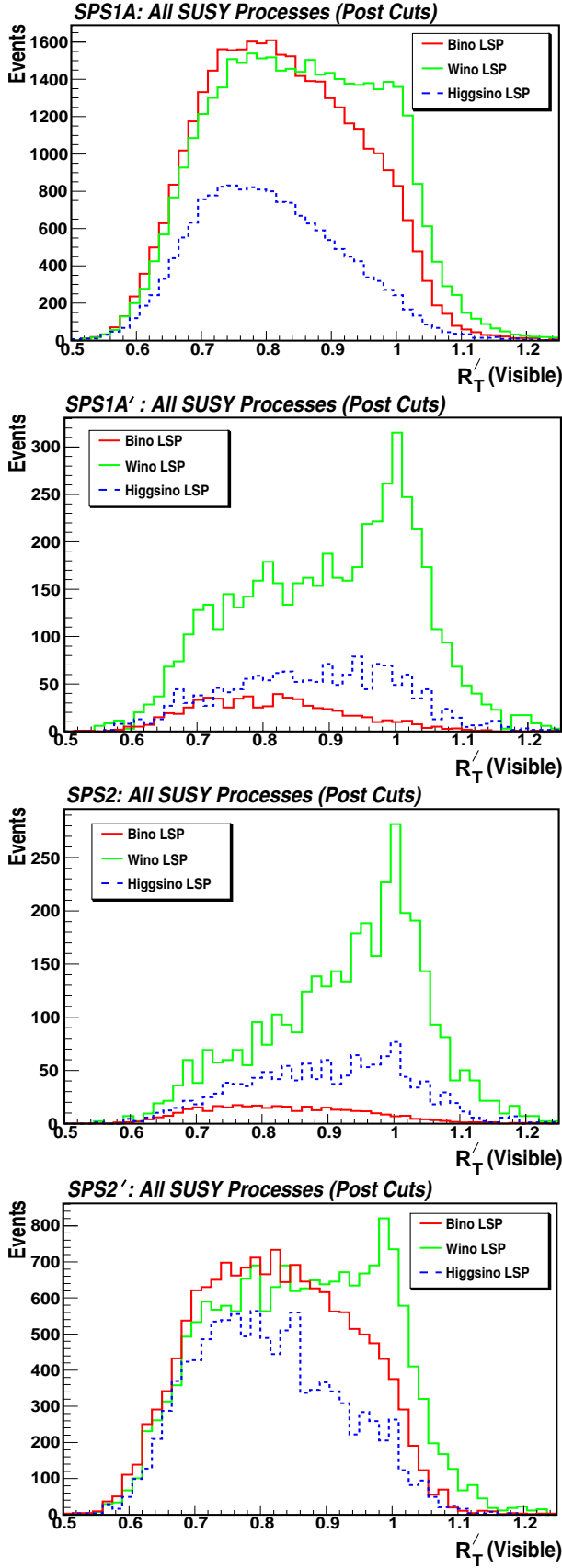


FIG. 5. Distribution of  $r'_T$  shape variable for SPS-based endpoint files, after the minimal cuts described in the text. Of particular importance is the requirement  $q_T < 0.35$  which isolates the signal region to  $r'_T \gtrsim 0.5$ . These distributions have been normalized to a constant integrated luminosity of  $10 \text{ fb}^{-1}$ .

Extreme	SPS 1A				SPS 2			
	All SUSY	SS	SG	GG	All SUSY	SS	SG	GG
Bino	41.48	39.99	1.42	0.15	1.76	1.38	0.04	0.32
Wino	63.07	39.97	2.32	20.88	23.87	1.38	0.06	22.36
Hino	49.98	39.28	0.33	10.39	11.29	1.38	0.01	9.85

TABLE VI. Production cross-sections for benchmark points SPS 1A and SPS 2. In addition to the total supersymmetric production cross-section we give breakdowns for strong-strong (SS) production, semi-strong production of an electroweak gaugino with a squark or gluino (SG) and electroweak gaugino pair production (GG). Cross-sections are in units of picobarns.

tion is still sufficient to upset the simple-minded arguments of Section II, but it will not prove fatal to our ability to make distinctions between wavefunction extremes using the shape variables of Section III.

We can use the variable  $q_T$ , together with kinematic cuts on missing transverse energy and transverse mass, to simultaneously diminish the Standard Model backgrounds while isolating as much as possible the semi-strong component of the  $r'_T$  distribution. In our analysis we will impose the following ‘minimal’ cuts: (1) require  $\cancel{E}_T \geq 175 \text{ GeV}$ , (2) require zero or one isolated lepton, (3) if one isolated lepton, form the transverse mass  $M_T$  of the lepton with the missing transverse energy and require  $M_T \geq 125 \text{ GeV}$ , (4) require  $q_T \leq 0.35$ . We plot the distribution in the remaining variable  $r'_T$ , after these minimal cuts are applied, for our benchmark models in Figure 5. These distributions are now normalized to a constant integrated luminosity of  $10 \text{ fb}^{-1}$ . The signal region is now well-defined as the region with  $r'_T \geq 0.5$  and the difference between the wave-function extremes is clear for all four benchmarks.

Inclusion of the Standard Model backgrounds, normalized to the same integrated luminosity, distorts these distributions, even after the imposition of the minimal cuts of the previous paragraph. For example, the upper panel of Figure 6 adds the Standard Model background sample to the SPS 1A distributions in the top panel of Figure 5. Much of the information contained in the shapes near  $r'_T \simeq 1$  is washed out by the large Standard Model contribution. Yet the minimal cuts can be easily augmented to recover discrimination in this variable. For example, the lower panel of Figure 6 increases the missing transverse energy cut to  $\cancel{E}_T \geq 250 \text{ GeV}$  and require the  $p_T$  of the leading jet to satisfy  $p_T^{\text{jet}} \geq 150 \text{ GeV}$ . The excess over the Standard Model in the region  $r'_T \geq 0.8$  is significant and the differences between the wave-function extremes is evident.

A quantitative measure of the power of the shape-variable method to distinguish between various LSP wavefunctions can be obtained from integrating the distributions in Figure 6 from some minimum value in  $r'_T$ . In Tables VII and VIII we integrate the tails of the  $r'_T$  distribution for three different minimum  $r'_T$  values for benchmark SPS 1A and SPS 2, respectively. For these tables the events were selected after applying the minimal cuts described above. For a given overall supersymmetric cross-section – as measured, for example,



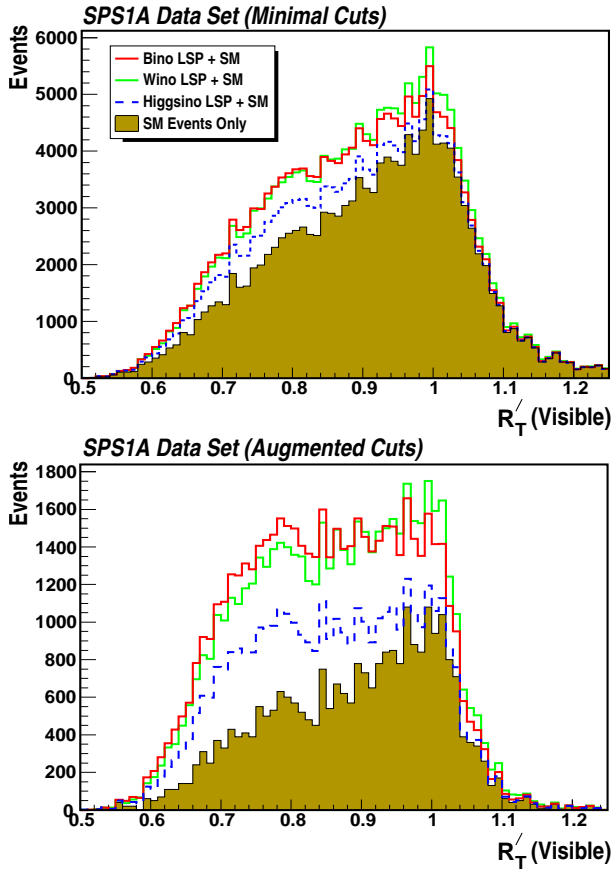


FIG. 6. Distribution of  $r'_T$  shape variable for SPS 1A with Standard Model contribution. The top panel is after the minimal cuts described in the text. The shaded region represents the SM background; the three curves represent the supersymmetric signal added to this background. The bottom panel is after ‘augmented’ cuts:  $p_T^{\text{jet}_1} > 150$  GeV and  $\cancel{E}_T > 250$  GeV. All distributions are normalized to a constant integrated luminosity of  $10 \text{ fb}^{-1}$ .

$r'_T$ Cut	Bino		Wino		Higgsino		SM Events
	Events	$S/\sqrt{B}$	Events	$S/\sqrt{B}$	Events	$S/\sqrt{B}$	
$r'_T \geq 0.8$	20,216	61.9	24,730	75.8	8,229	25.2	150,524
$r'_T \geq 1.0$	2,726	14.3	5,215	27.3	855	4.5	106,520
$r'_T \geq 1.1$	293	3.5	667	7.9	145	1.7	16,760

TABLE VII. Integrated counts and significances for SPS 1A. Normalized to  $10 \text{ fb}^{-1}$ .

by the inclusive counts of events with  $\cancel{E}_T \geq 500$  GeV or some other inclusive variable – the number of events with

$r'_T \geq (r'_T)_{\min}$  is clearly capable of distinguishing between the three LSP wavefunction extremes in the presence of the SM backgrounds. When cuts are optimized it is very likely that the goals of our analysis can be achieved for the full LSP wavefunction.

$r'_T$ Cut	Bino		Wino		Higgsino		SM Events
	Events	$S/\sqrt{B}$	Events	$S/\sqrt{B}$	Events	$S/\sqrt{B}$	
$r'_T \geq 0.8$	1,083	1.5	15,203	20.8	4,949	6.8	752,620
$r'_T \geq 1.0$	183	0.4	5,716	13.4	1,371	3.2	532,600
$r'_T \geq 1.1$	46	0.2	979	5.2	203	1.1	83,800

TABLE VIII. Integrated counts and significances for SPS 2. Normalized to  $50 \text{ fb}^{-1}$ .

## V. CONCLUSION

Should supersymmetry be discovered in the near future at the LHC the energies of the theoretical community will be directed towards an understanding of the properties of the superpartners and the parameters of the underlying supersymmetric Lagrangian. Few such quantities are of more general import than the wavefunction components of the lightest supersymmetric particle. In this paper we have taken a first step towards measuring this crucial property using inclusive data collected at the LHC. We have introduced new event-shape variables and demonstrated their ability to track changes in the contribution of sub-dominant SUSY production processes which are, in turn, sensitive to the wavefunction of the LSP. This work demonstrates the potential power of the technique, which is plainly evident from the analysis performed on four simple supersymmetric benchmark models. Here we have not tried to optimize the cuts imposed, nor sought full experimental realism. Instead we leave development of a full-fledged analysis algorithm to a future work. In particular, it would be of great value to analyze how such techniques fare in cases which interpolate between the wavefunction extremes considered here. Ultimately one might anticipate an algorithm that would serve as a quantitative measurement of the eigen-components  $N_{1i}$  of the neutralino mixing matrix robust enough to handle a variety of supersymmetric models.

## ACKNOWLEDGEMENTS

We would very much like to thank Michael Holmes for assistance in the early stages of this work. This research was supported by National Science Foundation Grants PHY-0653587 and PHY-0757959, and support from the Michigan Center for Theoretical Physics (MCTP) and Department of Energy grant DE-FG02-95ER40899.

- [2] P. Binetruy, G. L. Kane, J. D. Lykken and B. D. Nelson, J. Phys. G **32**, 129 (2006) [arXiv:hep-th/0509157].
- [3] B. Altunkaynak, P. Grajek, M. Holmes, G. Kane and B. D. Nelson, JHEP **0904**, 114 (2009) [arXiv:0901.1145 [hep-ph]].
- [4] H. Goldberg, Phys. Rev. Lett. **50**, 1419 (1983) [Erratum-ibid. **103**, 099905 (2009)].
- [5] A. Birkedal-Hansen and B. D. Nelson, Phys. Rev. D **64**, 015008 (2001) [arXiv:hep-ph/0102075].
- [6] A. Birkedal-Hansen and B. D. Nelson, Phys. Rev. D **67**, 095006 (2003) [arXiv:hep-ph/0211071].
- [7] O. Adriani *et al.* [PAMELA Collaboration], Nature **458**, 607 (2009) [arXiv:0810.4995 [astro-ph]].
- [8] O. Adriani *et al.*, Astropart. Phys. **34**, 1 (2010) [arXiv:1001.3522 [astro-ph.HE]].
- [9] G. L. Kane, L. T. Wang and T. T. Wang, Phys. Lett. B **536**, 263 (2002) [arXiv:hep-ph/0202156].
- [10] D. Feldman, G. Kane, R. Lu and B. D. Nelson, Phys. Lett. B **687**, 363 (2010) [arXiv:1002.2430 [hep-ph]].
- [11] M. Brhlik and G. L. Kane, Phys. Lett. B **437**, 331 (1998) [arXiv:hep-ph/9803391].
- [12] N. Arkani-Hamed, G. L. Kane, J. Thaler and L. T. Wang, JHEP **0608**, 070 (2006) [arXiv:hep-ph/0512190].
- [13] B. C. Allanach *et al.*, Eur. Phys. J. C **25**, 113 (2002) [arXiv:hep-ph/0202233].
- [14] V. Khachatryan *et al.* [CMS Collaboration], Phys. Lett. B **698**, 196 (2011) [arXiv:1101.1628 [hep-ex]].
- [15] G. Aad *et al.* [Atlas Collaboration], arXiv:1102.2357 [hep-ex].
- [16] J. B. G. da Costa *et al.* [Atlas Collaboration], arXiv:1102.5290 [hep-ex].
- [17] O. Buchmueller *et al.*, arXiv:1102.4585 [hep-ph].
- [18] T. Sjostrand, S. Mrenna and P. Z. Skands, JHEP **0605**, 026 (2006) [arXiv:hep-ph/0603175].
- [19] T. Gherghetta, G. F. Giudice and J. D. Wells, Nucl. Phys. B **559**, 27 (1999) [arXiv:hep-ph/9904378].
- [20] J. L. Feng and T. Moroi, Phys. Rev. D **61**, 095004 (2000) [arXiv:hep-ph/9907319].
- [21] F. E. Paige and J. D. Wells, arXiv:hep-ph/0001249.
- [22] V. D. Barger and R. J. N. Phillips, *Collider Physics*, Addison-Wesley, 1991.
- [23] H. Baer, C. h. Chen, F. Paige and X. Tata, Phys. Rev. D **52**, 2746 (1995) [arXiv:hep-ph/9503271].